S1 Estimation of the pure component viscosity of water

The pure component viscosity of water was estimated using the parameterization developed by Dehaoui et al. (2015) for all model simulations in this work; see Eq. (10) of main text. The experimental data used for developing the Dehaoui et al. (2015) parameterization extends from 239.15 K to 491.95 K. The parameterization is in excellent agreement with the data when temperatures are below $\sim$ 400 K. In Fig. S1, we compare the Dehaoui et al. (2015) parameterization with a parameterization by Viswanath et al. (2007) and with experimental data. The parameterization by Viswanath et al. (2007) is in better agreement with experimental data above $\sim$ 400 K when compared to the Dehaoui et al. (2015) parameterization. The Viswanath et al. (2007) parameterization is also in excellent agreement with the experimental data down to $\sim$ 270 K, below which it begins to deviate substantially from the available experimental data. Between 270 K and $\sim$ 380 K the two parameterizations are almost indistinguishable. Here we choose to use the Dehaoui et al. (2015) parameterization given that it is the more robust parameterization at lower temperatures of relevance in the troposphere.

S2 Exploration of the relationship between pure component vapour pressure and viscosity

In this study, initially an attempt was made to estimate the pure component viscosity of organic compounds from their pure component vapour pressures. The pure component viscosity is shown as a function of pure component vapour pressure in double logarithm space in Fig. S2. There is only a weak linear relationship between viscosity and vapour pressure when considering the range of viscosity from liquid to glassy for both the Nannoolal et al. (2008) and EVAPORATION model vapour pressure predictions. A stronger linear relationship exists in the liquid range, but below a vapour pressure of 10^{-5} Pa, the relationship between viscosity and vapour pressure becomes less clear and reliable data are scarce. We still hypothesize a relationship to exist between the two pure-component properties even in the semi-solid and glassy regimes. Although, it is likely
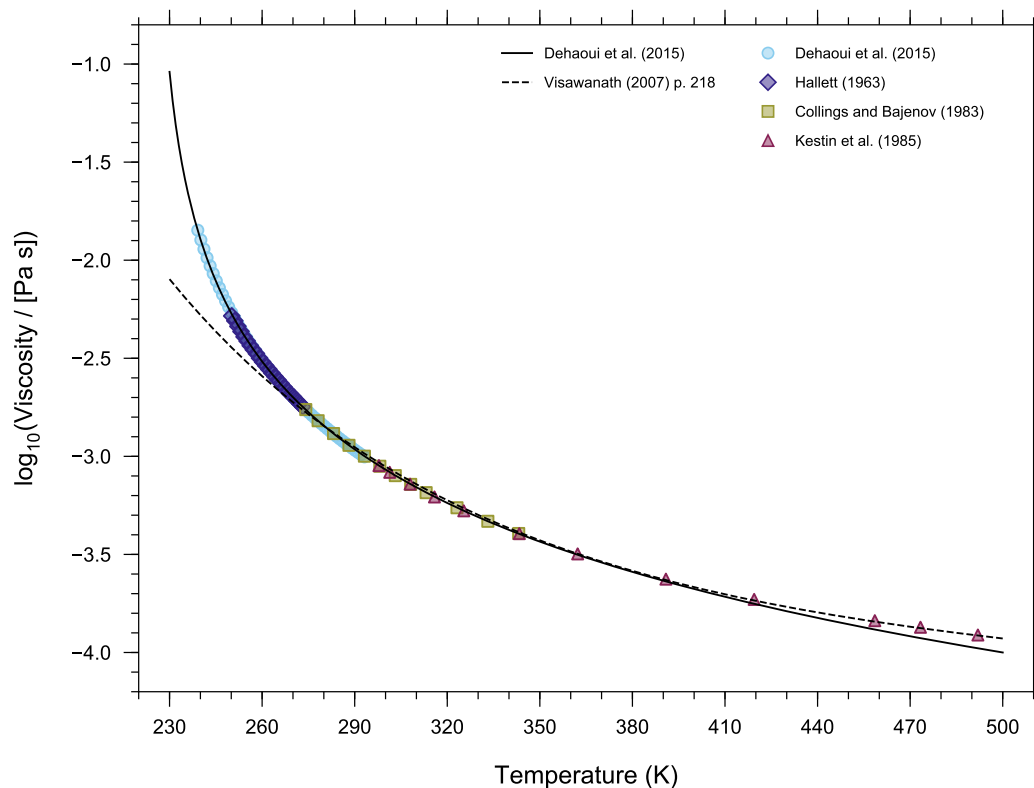
Figure S1. Parameterizations of the pure-component viscosity of water from Dehaoui et al. (2015) (solid line) and Viswanath et al. (2007) (dashed line). Markers represent experimental data where error bars have been omitted for clarity. The Dehaoui et al. (2015) parameterization is supported by measurements from $\sim$ 230 to 400 K and the Viswanath et al. (2007) parameterization is supported by measurements from $\sim$ 270 to 500 K.

this relationship is not resolved with the vapour pressure and viscosity estimation tools used here, given these tools have been trained with compounds that have higher vapour pressure and liquid viscosity only. Just as direct measurements of ultra-high pure-component viscosities are challenging to make, so too are measurements of ultra-low pure component vapour pressures. In order to fully elucidate the relationship between the two material properties, more precise experimental measurements are needed to better constrain pure-component property estimation tools.
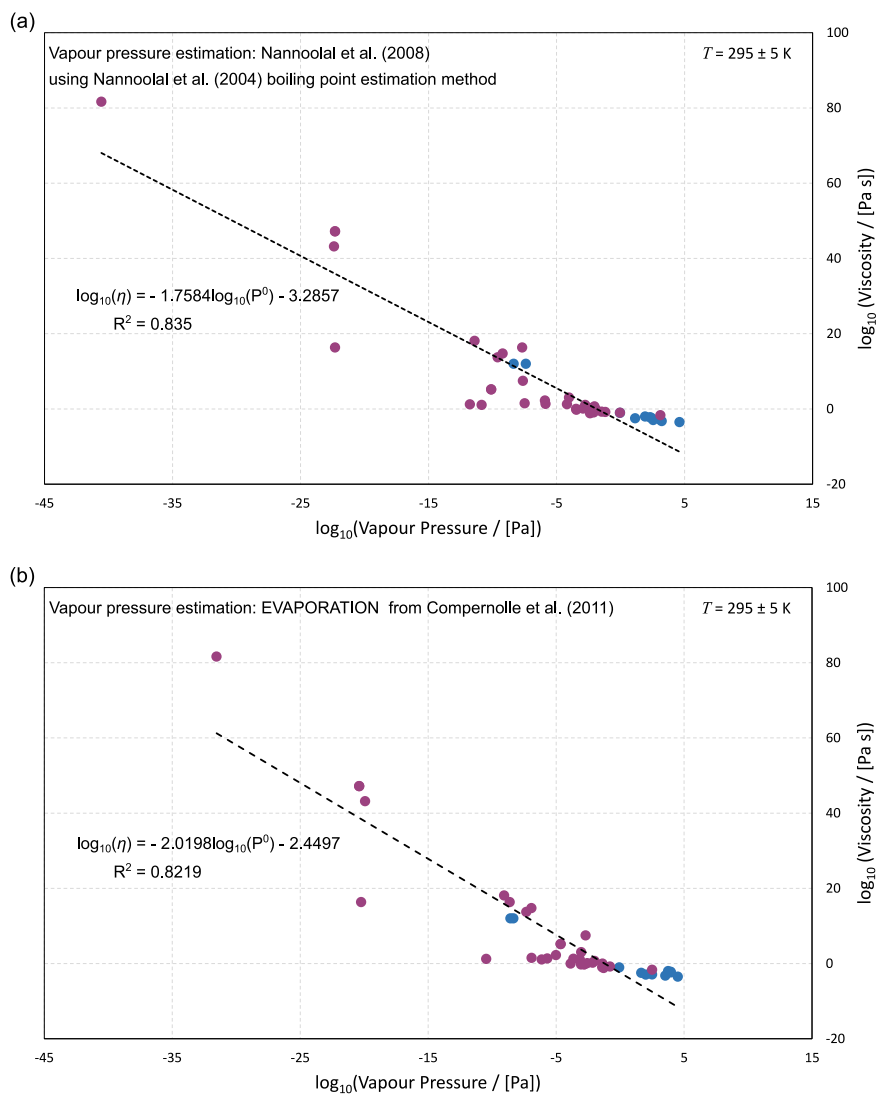
(a)

Vapour pressure estimation: Nannoolal et al. (2008)
using Nannoolal et al. (2004) boiling point estimation method

$T = 295 \pm 5$ K

$\log_{10}(\eta) = -1.7584\log_{10}(P^0) - 3.2857$

$R^2 = 0.835$

$\log_{10}$ (Viscosity / [Pa s])

$\log_{10}$(Vapour Pressure / [Pa])

(b)

Vapour pressure estimation: EVAPORATION from Compernolle et al. (2011)

$T = 295 \pm 5$ K

$\log_{10}(\eta) = -2.0198\log_{10}(P^0) - 2.4497$

$R^2 = 0.8219$

$\log_{10}$ (Viscosity / [Pa s])

$\log_{10}$(Vapour Pressure / [Pa])

Figure S2. Reference or modelled pure component viscosity as a function of modelled pure component vapour pressure. Vapour pressures have been estimated using (**a**) the online tool UManSysProp (http://umansysprop.seaes.manchester.ac.uk) with the Nannoolal et al. (2008) vapour pressure model and the Nannoolal et al. (2004) boiling point estimation method and (**b**) the EVAPORATION model (Compernolle et al., 2011). Purple markers indicate values where the viscosity has been modelled using the method by Nannoolal et al. (2009). Blue markers indicate reference viscosity values either from direct experimental measurements or from an extrapolation with the Vogel–Tamman–Fulcher equation to $T = 293.15$ K using pure-component viscosity values measured at higher temperatures. All model values have been calculated at 293.15 K. Reference viscosity values are taken at a range of temperatures (295 ± 5 K). Dashed black lines indicate linear regressions (in logarithm space) to the combined reference and model data.

Table S1. Measured, parameterized, or modelled values of the glass transition temperature (T_g) from the literature. Uncertainty values are listed when they are provided from their source.

Compound	T_g (K)	Reference	Compound	T_g (K)	Reference
1,2,4-Butanetriol	200.7	Nakanishi and Nozaki (2011)	Glycerol	187	Angell (1997)
1,2,6-Hexanetriol	202	Böhmer et al. (1993)		193	Angell (1997)
	206.4 ± 0.5	Dorfmüller et al. (1979)		190	Böhmer et al. (1993)
	201.9	Nakanishi and Nozaki (2011)		191 ± 0.9	Lienhard et al. (2012)
	192 ± 2	Zhang et al. (2018)		191.7	Nakanishi and Nozaki (2011)
	193.3 ± 1.3	Zobrist et al. (2008)		196	Seidl et al. (2013)
1,4-Butanediol	158.4 ± 1.1	Zobrist et al. (2008)		192 ± 2	Zhang et al. (2018)
Citric Acid	281 ± 5	Bodsworth et al. (2010)	Raffinose	377.9 ± 0.9	Lienhard et al. (2012)
	286 ± 1.5	Dette et al. (2014)		395.7 ± 21.6	Zobrist et al. (2008)
	273.25 ± 3.4	Hoppu et al. (2009)	Sorbitol	266	Angell (1997)
	281.9 ± 0.9	Lienhard et al. (2012)		274	Böhmer et al. (1993)
	284.15 ± 0.2	Lu and Zografi (1997)		268.3	Nakanishi and Nozaki (2011)
	286 ± 10	Marsh et al. (2018)		276^{mid}	Simatos et al. (1996)
	260 ± 10	Murray (2008)	Sucrose	323	Angell (1997)
	$283.35^{in\ situ}$	Timko and Lordi (1979)		331 ± 2	Dette et al. (2014)
	286.65^{bulk}	Timko and Lordi (1979)		350 ± 3.5	Hancock et al. (1995)
	307 ± 5	Zhang et al. (2018)		341	Kawai et al. (2005)
Fructose	283.15	Ablett et al. (1993)		341	Rothfuss and Petters (2017)
	286	Angell (1997)		333^{mid}	Simperler et al. (2006)
	283	Ollet and Parker (1990)		$347^{calculated}$	Simperler et al. (2006)
	289^{mid}	Simatos et al. (1996)		335.7 ± 3.6	Zobrist et al. (2008)
Glucose	306	Angell (1997)	Trehalose	388	Angell (1997)
	297 ± 2	Dette et al. (2014)		369 ± 1.5	Dette et al. (2014)
	309	Kawai et al. (2005)		386	Kawai et al. (2005)
	293.2 ± 0.9	Lienhard et al. (2012)		380^{mid}	Simperler et al. (2006)
	304	Ollet and Parker (1990)		$392^{calculated}$	Simperler et al. (2006)
	296^{mid}	Simperler et al. (2006)			
	$325^{calculated}$	Simperler et al. (2006)			
	296.1 ± 3.1	Zobrist et al. (2008)			

S3 Estimation of AIOMFAC-VISC sensitivity

We calculated the sensitivity of AIOMFAC-VISC as a proxy for the uncertainty in the mixture viscosity prediction. We chose to prescribe the AIOMFAC-VISC sensitivity as the response of the mixture viscosity prediction to a small change in mixture composition. A small change in mixture composition is meant to represent the uncertainty in the composition measurement in a laboratory setting, which would be typical of all experiments. Therefore, the AIOMFAC-VISC sensitivity of mixture viscosity, s_η, is calculated using a molar partial derivative:

$$s_\eta = x^{\text{tol}} \left[\frac{\partial \ln(\eta_{\text{mix}})}{\partial n_{\text{H}_2\text{O}}} \right] \tag{S1}$$

where x^{tol} is the molar tolerance (the prescribed uncertainty) in the mixture composition. To retrieve x^{tol} we first perturb the mass of water by $\delta_m = 2\ \%$ of the mass of the total system,

$$m_{\text{H}_2\text{O}} = m_{\text{H}_2\text{O,init}} + \delta_m, \tag{S2}$$

where $m_{\text{H}_2\text{O,init}}$ is the initial mass of water in the mixture (e.g. $m_{\text{H}_2\text{O,init}} = w_{\text{H}_2\text{O,init}}$ for 1 kg of total mass of the mixture) and $m_{\text{H}_2\text{O}}$ is the perturbed mass. Next, the mass fractions of all components are normalized to account for the mass addition via

$$w_i = \frac{w_{i,\text{init}}}{1 + \delta_m}, \tag{S3}$$

where w_i represents the normalized mass fraction of a given component i given the initial mass fraction $w_{i,init}$. By doing this, we prescribe the model sensitivity as strictly a change in water content of the mixture, where the mixing ratio of organic constituents remains fixed. The normalized mass fractions are then converted to mole fractions (x_i) and finally, x^{tol} is calculated as the difference between the mole fractions of the perturbed system and the unperturbed system.

$$x^{\text{tol}} = x_{\text{H}_2\text{O}} - x_{\text{H}_2\text{O,init}}. \tag{S4}$$

S4 Comparison of AIOMFAC-VISC and GC-UNIMOD

Here we compare the performance of the mixture viscosity prediction of AIOMFAC-VISC with the original Cao et al. (1993), GC-UNIMOD model. To compare the mixture viscosity prediction absent of uncertainty introduced by the pure-component viscosity prediction, we have fixed the pure-component viscosity of citric acid to a fitted value at the temperature of interest here (as described in the main text) and we have used the experimental pure-component viscosity of glycerol. As seen in Fig. S3 the AIOMFAC-VISC mixture viscosity prediction is greatly improved from that by the GC-UNIMOD model. The same behaviour was observed for the other binary aqueous mixtures investigated in this work.
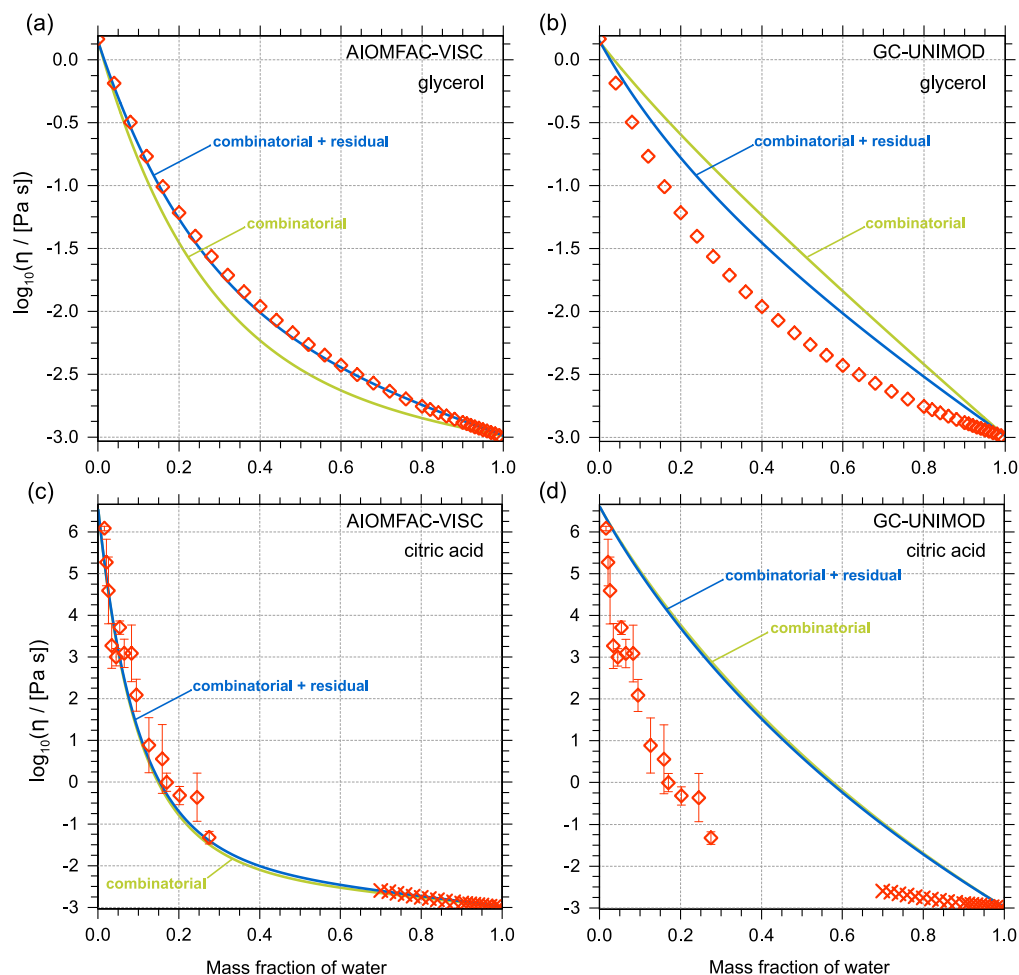
Figure S3. A comparison of predicted mixture viscosity as a function of mass fraction of water shown for glycerol (top two panels) and citric acid (bottom two panels). The blue curves represent mixture viscosity computed with both combinatorial and residual contributions. The yellow curves represent computations using combinatorial mixture viscosity only. The AIOMFAC-VISC mixture viscosity prediction for glycerol (**a**) and citric acid (**c**) is in significantly better agreement with the experimental data (red markers) as compared to the GC-UNIMOD mixture viscosity prediction for both glycerol (**b**) and citric acid (**d**). The changes made to the combinatorial viscosity contribution from GC-UNIMOD to AIOMFAC-VISC account for most of the improvement.

S5 Binary aqueous mixture viscosity predictions for all training data

To optimize the mixing model of AIOMFAC-VISC, we attempted to simultaneously fit the mixing model prediction to experimental viscosity data for the binary aqueous mixtures shown in Figs. S4, S5, and S6. The fit is captured by an adjustable parameter multiplied by the residual component of the mixture viscosity model. The determination of an optimal fit parameter is a global minimization problem, ideally approached by using a set of global optimization methods. For this, we used the optimization approach described by Zuend et al. (2011). The optimal fit parameter was determined to be ~ 1.0, therefore no further adjustments were made to the mixture viscosity model aside from those adjustments made to the original Cao et al. (1993) formulation described in the main text.

S6 Determination of SOA systems

For all three SOA systems simulated in this work, each surrogate compound was assigned a fixed molar concentration in the particulate matter (PM). These fixed molar concentrations in $\mathrm{mol\,m^{-3}}$ (of air) are listed in Tables S2, S3, and S4 for α-pinene-, toluene-, and isoprene-derived SOA, respectively. To determine those molar concentration of constituents for the α-pinene and isoprene SOA systems, we begin by calculating the equilibrium gas–particle partitioning of the surrogate species in each SOA system using the MCM–EVAPORATION–AIOMFAC approach (Zuend et al., 2011) where the initial total molar concentrations (PM plus gas phase) for α-pinene and isoprene SOA were taken from Zuend and Seinfeld (2012) and Rastak et al. (2017), respectively. We extract the molar concentration of each constituent in the PM phase for a relative humidity of $40\,\%$. When relative humidity is held at $40\,\%$, the average $\mathrm{O:C}$ ratio of the SOA produced via our gas–particle partitioning prediction is representative of known $\mathrm{O:C}$ ratios from experiments. We then hold the molar concentrations of organics in the PM constant during calculations of mixture viscosity. In the case of α-pinene SOA, we have made one additional adjustment by scaling the molar amount of surrogate compound C108OOH in the PM phase by a factor of 30. This is done to better match the curvature of the experimental viscosity data at high relative humidity. In the case of toluene SOA, we have selected several constituents from the MCM-derived list of surrogate components from toluene photo-oxidation by OH radicals. To determine the molar concentrations of a given constituent (n_i) in the PM phase we use the following formula:

$$n_i = \mathrm{O:C} \times T_{\mathrm{g}} \times 10^{-10}. \tag{S5}$$

Using this scaling results in the $\mathrm{O:C}$ of the SOA produced to be similar to what is expected from laboratory chamber experiments. We note here that we have increased the concentration of compound C535OOH by a factor of 5 to increase the average mixture O:C from 0.96 to 1.12.

It is important to note that AIOMFAC-VISC predictions are relatively sensitive to adjustments made to the average $\mathrm{O:C}$ ratio, which is a reflection of the sensitivity of the model to changes in SOA composition. Figure S7 demonstrates the changes to mixture viscosity over a plausible range of average $\mathrm{O:C}$ values. However, we note that the used variations in a mixture's average $\mathrm{O:C}$ ratio are imposed here for the purpose of illustration. They are not the results of predictions by a chemical mechanism under different oxidation regimes and as such do not represent equally likely outcomes. As in Fig. 7 in the main
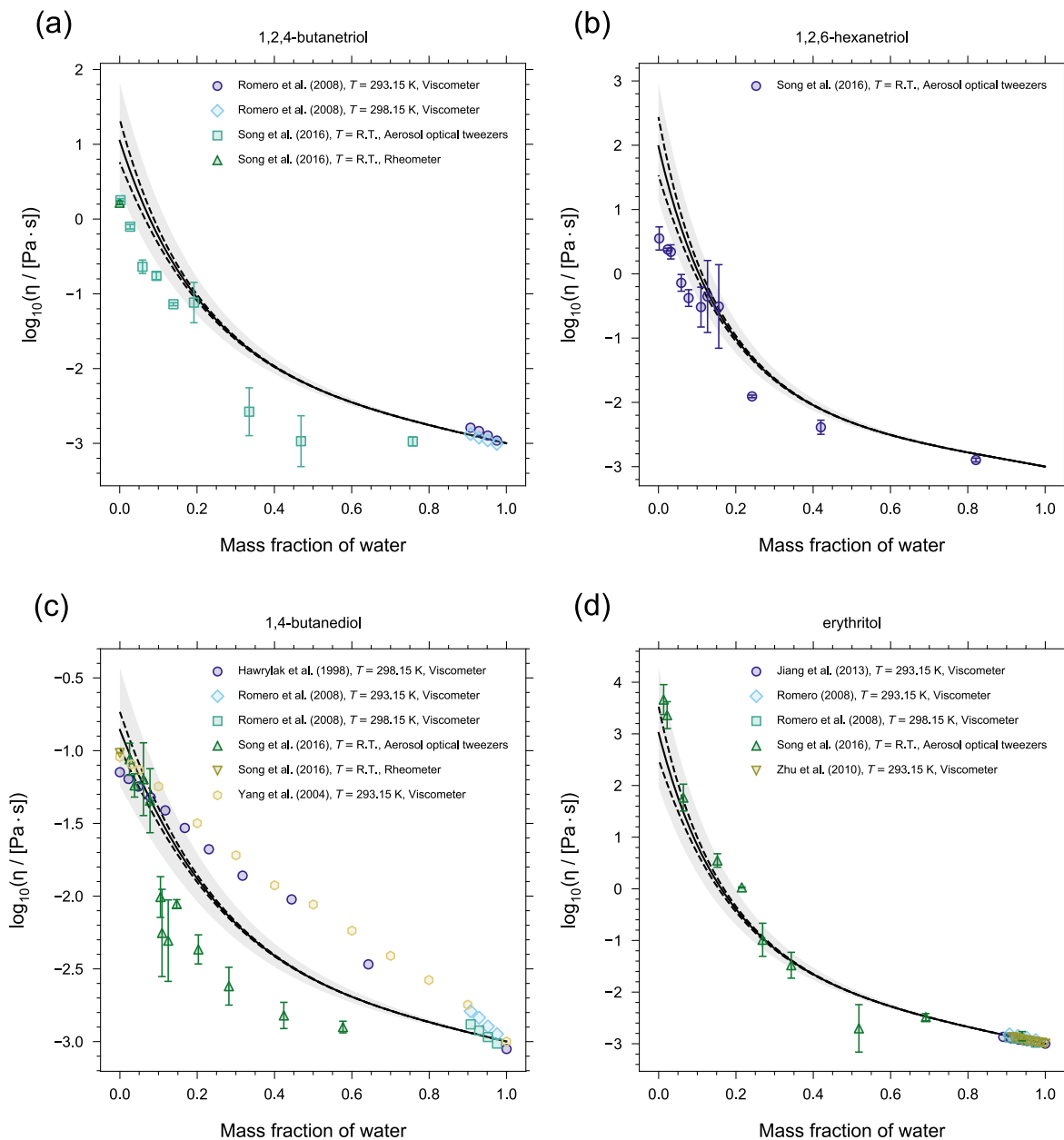
Figure S4. AIOMFAC-VISC mixture viscosity predictions as a function of mass fraction of water at 293.15 K for (**a**) 1,2,4-butanetriol, (**b**) 1,2,6-hexanetriol, (**c**) 1,4-butanetriol, and (**d**) erythritol. The solid black line is the AIOMFAC-VISC mixture viscosity prediction. The dashed black lines show the AIOMFAC-VISC sensitivity. The sensitivity is assessed by calculating the response of the model to a small change in mixture composition. The grey shaded region denotes a 5 % uncertainty in the prediction of T_g. Markers show experimental data. Error bars have been omitted when the length of the error bar does not exceed the width of the marker.
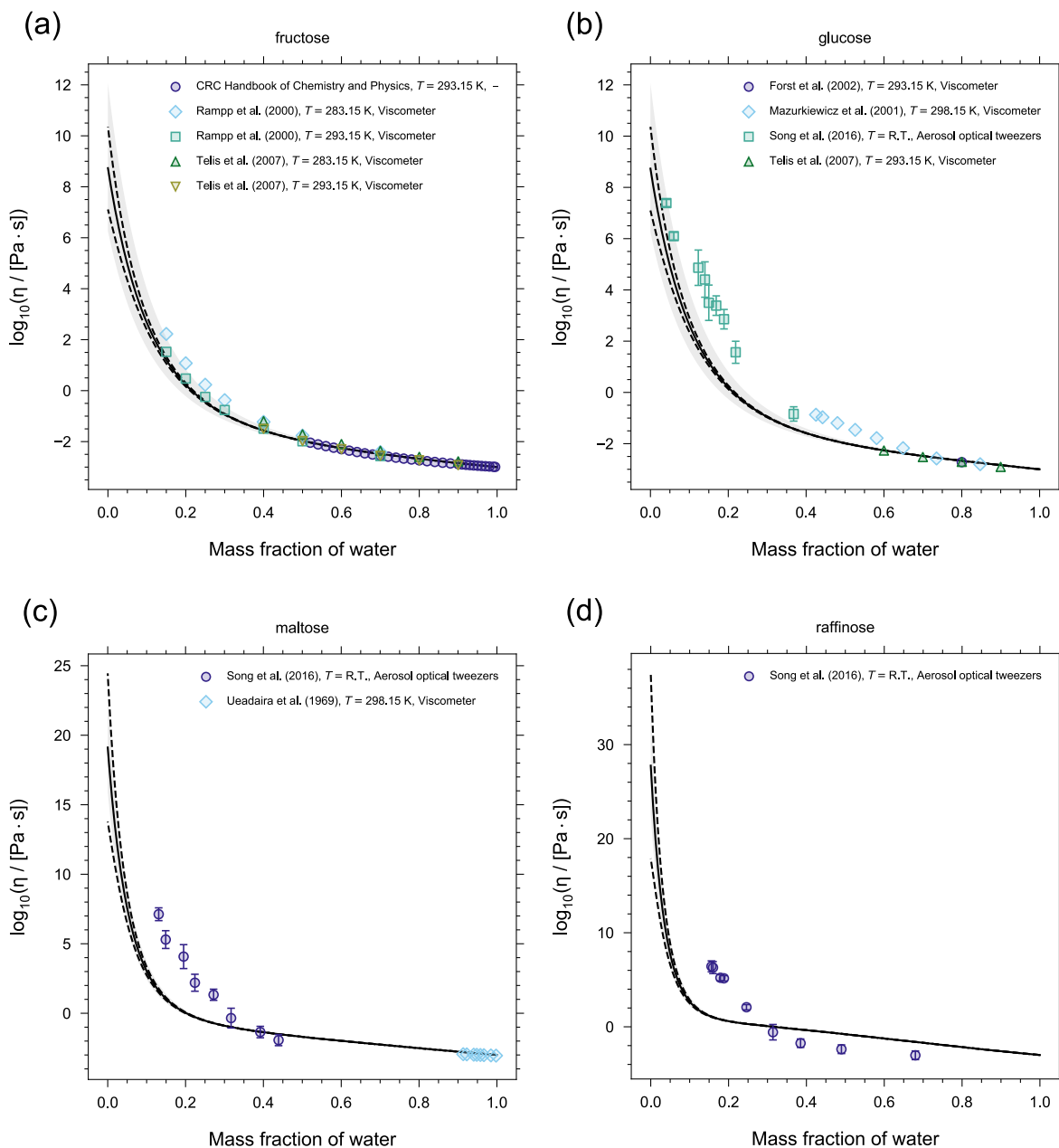
Figure S5. AIOMFAC-VISC mixture viscosity predictions as a function of mass fraction of water at 293.15 K for (**a**) fructose, (**b**) glucose, (**c**) maltose, and (**d**) raffinose. The solid black line is the AIOMFAC-VISC mixture viscosity prediction. The dashed black lines show the AIOMFAC-VISC sensitivity. The sensitivity is assessed by calculating the response of the model to a small change in mixture composition. The grey shaded region denotes a 5 % uncertainty in the prediction of T_g. Markers show experimental data. Error bars have been omitted when the length of the error bar does not exceed the width of the marker.

Figure S6. AIOMFAC-VISC mixture viscosity predictions as a function of mass fraction of water at 293.15 K for (**a**) acetic acid, (**b**) glutaric acid, (**c**) maleic acid, and (**d**) sorbitol. The solid black line is the AIOMFAC-VISC mixture viscosity prediction. The dashed black lines show the AIOMFAC-VISC sensitivity. The sensitivity is assessed by calculating the response of the model to a small change in mixture composition. The grey shaded region denotes a 5 % uncertainty in the prediction of T_g. Markers show experimental data. Error bars have been omitted when the length of the error bar does not exceed the width of the marker.
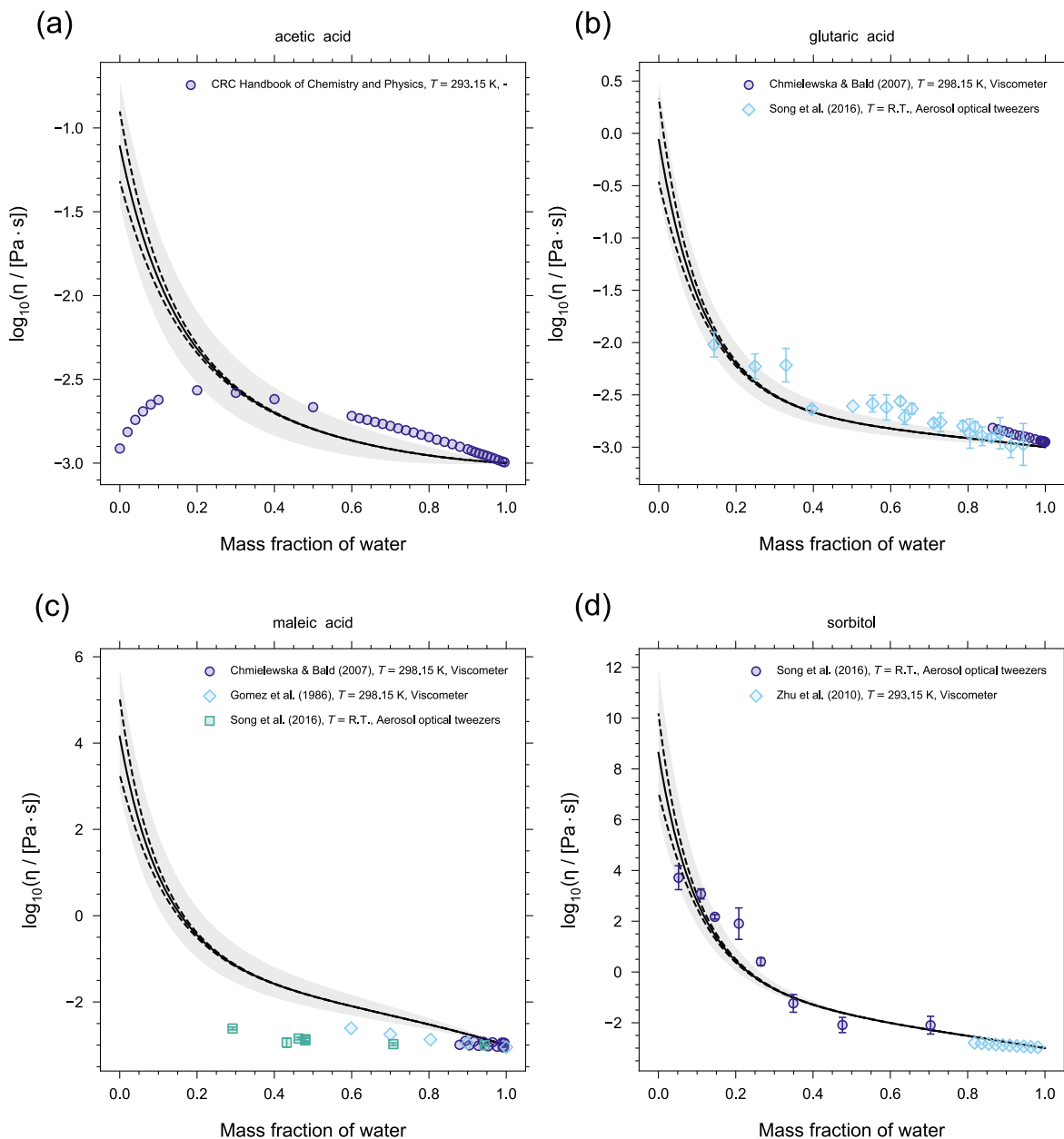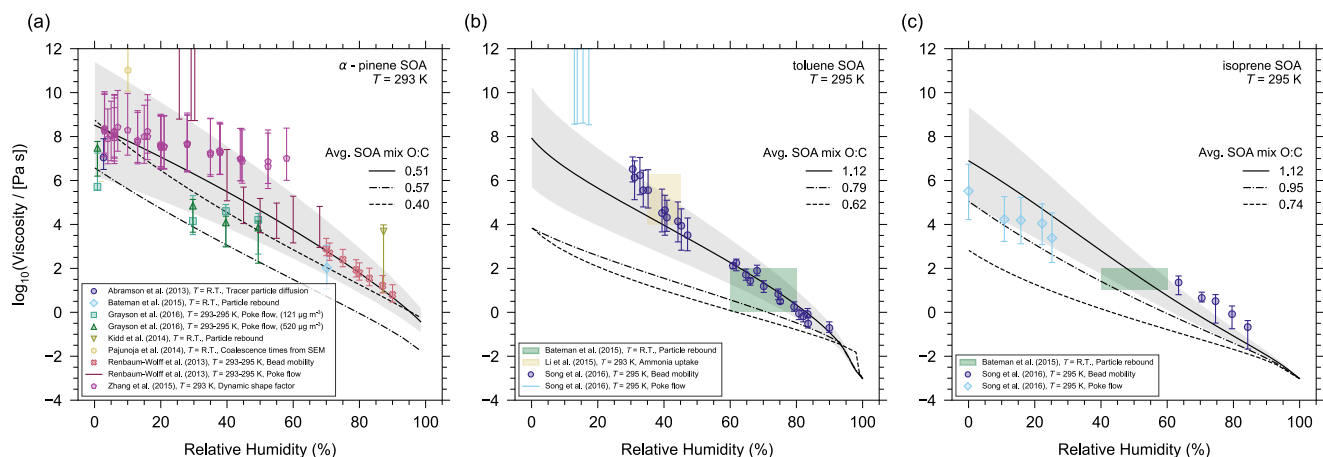
Figure S7. AIOMFAC-VISC mixture viscosity predictions for (**a**) α-pinene SOA at $T = 293$ K, (**b**) toluene SOA at $T = 295$ K, and (**c**) isoprene SOA at $T = 295$ K. The solid lines and the grey shaded regions represent the model results and their associated $5\,\%$ uncertainty in estimated T_{g} values from Fig. 7 of the main text. The dashed lines and dashed-dotted lines show AIOMFAC-VISC mixture viscosity for different average $\mathrm{O:C}$ for each SOA mixture. The markers and colour shaded regions represent experimental data obtained by different methods (see legend). $T = \mathrm{R.T.}$ indicates the measurements were taken at room temperature ($\sim 293 \pm 4$ K).

text, the relative contributions of the different organics were adjusted to change the average SOA $\mathrm{O:C}$. The changes in mixture composition brought about from the $\mathrm{O:C}$ adjustments are responsible for the differences in the model results. First, the mixture composition influences the curvature of the mixture viscosity prediction vs. RH. Second, the change in the relative contributions of the pure-component viscosities scales the mixture viscosity end point at $0\,\%$ RH.

5   AIOMFAC-VISC has proven to be very sensitive to mixture composition, which demonstrates that the model is flexible enough to reflect the viscosity of SOA formed under various experimental conditions. This is clear for the case of α-pinene (Fig. S7a) where the spread of experimental data is similar in magnitude to the spread in model results from varying mixture composition.

Table S2. MCM-derived surrogate components for alpha-pinene oxidation by ozone and their fixed amounts in $\mathrm{mol\,m^{-3}}$ in the particulate matter (PM) phase.

Name (MCM)	O:C	M (g mol^{-1})	$\mathrm{mol\,m^{-3}}$ in PM phase
C107OOH	0.4	200.231	2.1860×10^{-10}
PINONIC	0.3	184.232	1.2356×10^{-10}
C97OOH	0.44	188.22	2.5175×10^{-9}
C108OOH	0.5	216.231	8.4010×10^{-8}
C89CO2H	0.33	170.206	2.010×10^{-11}
PINIC	0.444	186.205	8.0263×10^{-9}
C921OOH	0.56	204.220	9.2106×10^{-9}
C109OOH	0.4	200.231	1.5748×10^{-11}
C812OOH	0.625	190.194	8.4291×10^{-9}
HOPINONIC	0.4	200.232	2.3266×10^{-9}
C811OH	0.375	158.094	8.9370×10^{-11}
C813OOH	0.75	206.193	3.2969×10^{-9}
ALDOL dimer	0.375	368.421	5.9996×10^{-10}
ESTER dimer	0.375	368.421	2.3998×10^{-9}

The ALDOL dimer and ESTER dimer are not predicted by MCM. Justification for including the dimers can be found in Zuend and Seinfeld (2012).

The average O:C ratio of the predicted α-pinene SOA mixture is 0.507 (for 27.248 µg m^{-3} of SOA formed at $T = 293.15$ K).

Table S3. MCM-derived surrogate components for toluene oxidation by OH and their fixed amounts in $\mathrm{mol\,m^{-3}}$ in the particulate matter (PM) phase.

Name (MCM)	O:C	M (g mol^{-1})	mol m^{-3} in PM phase
C5134CO2OH	0.8	130.099	1.9868×10^{-8}
C5CO234	0.6	114.099	1.3525×10^{-8}
PMALNHY2OH	0.714	174.151	1.9267×10^{-8}
C6H5CH2OOH	0.286	124.137	5.8337×10^{-9}
CRESOOH	0.857	190.151	2.4241×10^{-8}
TLEPOXMUC	0.429	140.137	1.9987×10^{-8}
MALANHY	0.75	98.057	1.6884×10^{-8}
C3DIALOOH	1.333	104.062	3.0168×10^{-8}
C33CO	1.0	86.046	2.2626×10^{-8}
C23O3CCHO	0.8	130.099	1.9868×10^{-8}
C535OOH	1.4	180.113	2.0366×10^{-7}
C534OOH	1.4	180.113	4.0863×10^{-8}

The average O:C ratio of the predicted toluene SOA mixture is 1.12 (for 301 µg m^{-3} of SOA formed at $T = 295.15$ K).

Table S4. MCM-derived surrogate components for isoprene photo-oxidation and their fixed amounts in $\mathrm{mol\,m^{-3}}$ in the particulate matter (PM) phase.

Name (MCM)	O:C	M (g mol^{-1})	$\mathrm{mol\,m^{-3}}$ in PM phase
IEB1OOH	1.0	150.1120	2.1859×10^{-9}
IEB2OOH	1.0	150.1120	3.8058×10^{-11}
C59OOH	1.0	150.0940	6.4468×10^{-9}
IEC1OOH	1.0	150.0940	2.2503×10^{-9}
C58OOH	1.0	150.1120	2.2710×10^{-10}
IEPOXA	0.6	118.1308	1.6303×10^{-31}
C57OOH	1.0	150.1120	1.8452×10^{-10}
IEPOXC	0.6	118.1308	3.7912×10^{-21}
HIEB1OOH	1.2	166.1120	2.3492×10^{-9}
INDOOH	1.4	197.1380	1.6072×10^{-9}
IEACO3H	1.0	148.0960	1.8935×10^{-19}
C525OOH	1.2	166.0940	1.7850×10^{-9}
HIEB2OOH	1.2	166.1120	1.0495×10^{-9}
IEC2OOH	1.0	148.0600	2.0814×10^{-17}
INAOOH	1.4	197.1380	7.2618×10^{-10}
C510OOH	1.4	195.1040	5.5325×10^{-13}
INB1OOH	1.4	197.1380	4.6077×10^{-10}
IECCO3H	1.0	148.1148	1.2558×10^{-17}
INCOOH	1.4	197.1380	8.7075×10^{-11}
INB2OOH	1.4	197.1380	1.8653×10^{-10}
Tetrol dimer	1.43	254.2768	3.9110×10^{-18}

The average O:C ratio of the predicted isoprene SOA mixture is 1.12 (for $3.406\,\mathrm{\mu g\,m^{-3}}$ of SOA formed at $T = 295.15$ K). See the SI of Rastak et al. (2017) for chemical formulas and justification for the tetrol dimer.

S7 AIOMFAC-VISC and the mole-fraction-based mixing rule for viscosity of binary aqueous and SOA systems

As detailed in the main text, the simple, mole-fraction-weighted mixing rule is the most competitive model that was explored for accurately capturing mixture viscosity of aqueous systems when compared to AIOMFAC-VISC. To quantitatively compare the two mixing rules, their mean absolute error (MAE) and mean bias error (MBE) as compared to binary aqueous experimental data are shown in Table S5. The MAE and the MBE are calculated as,

$$\text{MAE} = \frac{1}{N}\sum_{i=1}^{N}|\log_{10}(y_i + \delta_{x_i}) - \log_{10}(x_i + \delta_{x_i})| \quad ; \quad \text{MBE} = \frac{1}{N}\sum_{i=1}^{N}[\log_{10}(y_i + \delta_{x_i}) - \log_{10}(x_i + \delta_{x_i})]. \tag{S6}$$

Here, N is the number of data points in a given data set, y are the mixing model predictions of viscosity corresponding to the mixture composition of the experimental data and x are the experimental mixture viscosity data. The MAE and MBE are weighted by δ_{x_i}, which quantifies the measurement error or, if not available, the model sensitivity (see S3).

The MAE and MBE are shown in Table S5 for both mixing models when the pure-component viscosity is assigned as the highest confidence ("best") value. The highest confidence pure-component viscosity values are either taken from experiment, extrapolated from viscosity measurements very close to 0.0 mass fraction of water, or parameterizations of T_g in good agreement with experimental data (see Fig. 4 of the main text and Fig. S8). Comparing the sums of all system MAE and MBEs, when the highest confidence pure-component viscosities have been used, the mole-fraction scaled mixing rule has a slightly lower MAE and MBE. In the case of AIOMFAC-VISC, these cumulative metrics are dominated by relatively large MAE and MBE contributions from the aqueous sugar solution systems (raffinose, trehalose, maltose). These larger deviations from measurements are in part explained by the known deviations of AIOMFAC/UNIFAC water activity predictions from measurements for sugar-containing solutions. Therefore, the activity deviations impact the skill of AIOMFAC-VISC in predicting viscosity, while the mole-fraction-based mixing rule is not affected and provides the better mixture viscosity model for these systems. Notwithstanding, while the sums provide an overall comparison of the two models, they should be interpreted with caution, because large errors in case of some systems dominates the totals. An alternative and perhaps more insightful method to evaluate the two models is to compare them on a system-by-system basis. In this manner, the fraction of times AIOMFAC-VISC outperforms the mole-fraction scaled mixing rule is 61% in terms of MAE and 67% in terms of MBE when using the highest confidence pure-component viscosities. This indicates that AIOMFAC-VISC performs better particularly when uncertainties in the composition–activity relationship considered by the model do not dominate the model–measurement deviations.

Using the highest confidence pure-component viscosities offers the most direct statistical comparison of the two mixing rules; however, the MAE and MBE are also shown using the DeRieux et al. (2018) based pure-component viscosity estimation, given that this tool is used in practice in the current AIOMFAC-VISC framework. When using the DeRieux et al. (2018) method, AIOMFAC-VISC is the better performing model only in 24% of the cases in terms of MAE and 36% in terms of MBE. This is the case because the tendency of a high-bias in pure-component viscosity predictions by the DeRieux et al. (2018) (for the systems tested here) favours the mole-fraction scaled mixing rule (but not necessarily for the right reason). The discrepancy in model performance when using different pure-component viscosity estimation methods further highlights the need for an accurate pure-component viscosity prediction and supports further research to improve such models. Finally,

both AIOMFAC-VISC and the mole-fraction scaled mixing rule are clearly better than the activity-scaled mixing rule in approximately 91% of cases. Given the clear difference in performance of the activity-scaled mixing rule, compared to the other two models, the results of a detailed statistical analysis were not listed in Table S5 as it is not a recommended mixing rule.

5   For SOA systems, the AIOMFAC-VISC and the mole-fraction scaled mixing rule also give similar results (see Fig. S9). For α-pinene, the mole-fraction-weighted mixing rule overestimates the mixture viscosity at high relative humidity as compared to the AIOMFAC-VISC agreement with the data from Renbaum-Wolff et al. (2013). However, below approximately 50% RH, the model results are nearly identical. For toluene, AIOMFAC-VISC is in slightly better agreement with the experimental data, although the opposite is true for isoprene. Again, both models are very similar and the large spread in experimental

10   SOA data makes it difficult to compare the performance of the models conclusively. Both models are viable for mixture viscosity prediction and the mole-fraction-weighted mixing rule provides a robust alternative to AIOMFAC-VISC, particularly for aqueous systems exhibiting orders of magnitude change in viscosity with composition. Ultimately, we note that only a small number of binary aqueous and multicomponent SOA systems were tested here, and when more experimental data of atmospheric relevance becomes available, further model evaluations can be performed. At present, the choice to use either
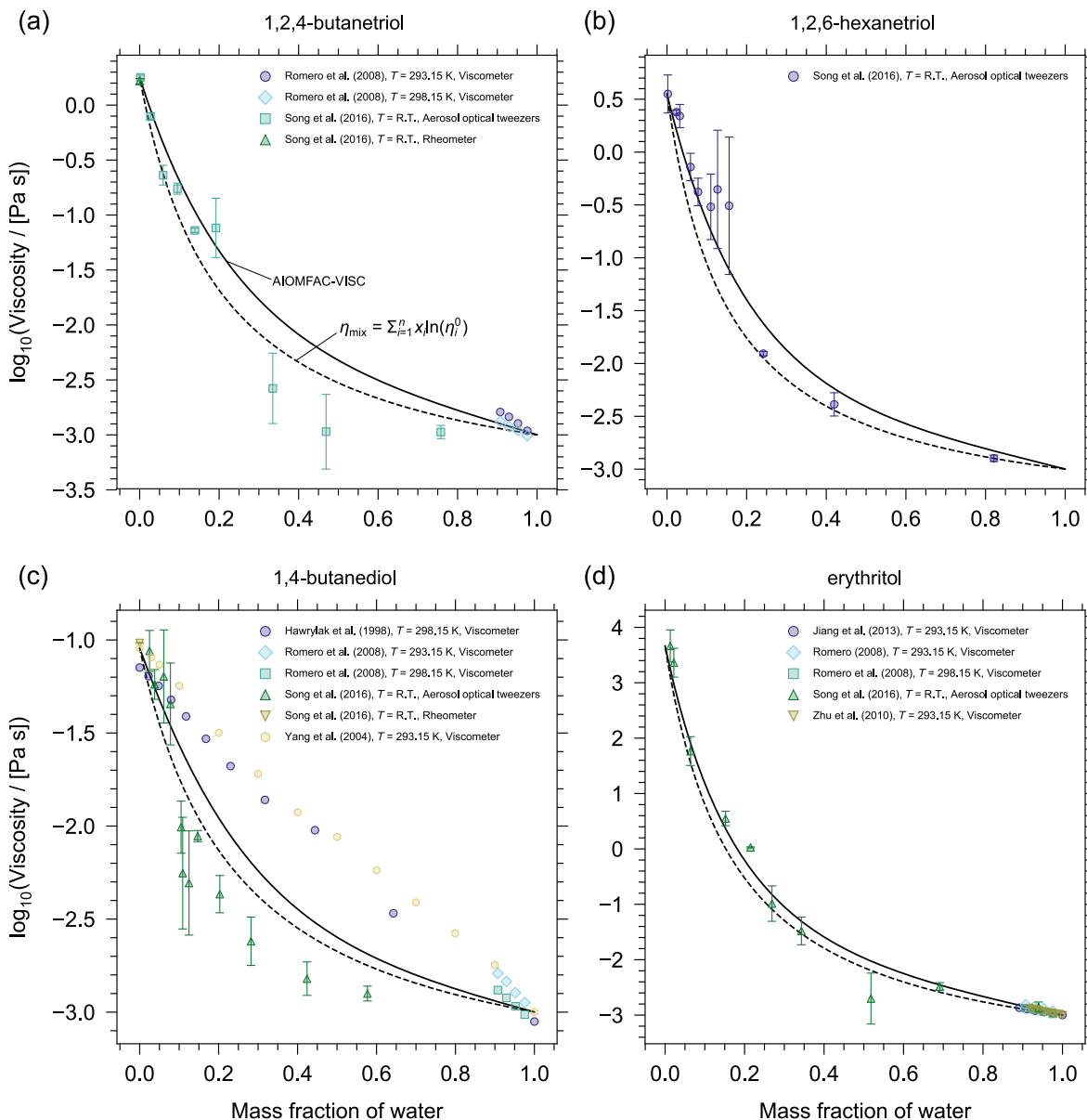
15   model can be made on a system-by-system basis.

Figure S8. AIOMFAC-VISC mixture viscosity predictions as a function of mass fraction of water at 293.15 K for (**a**) 1,2,4-butanetriol, (**b**) 1,2,6-hexanetriol, (**c**) 1,4-butanetriol, and (**d**) erythritol. The solid black lines are the AIOMFAC-VISC mixture viscosity prediction. The dashed black lines are the mixture viscosity prediction from the mole-fraction-weighted mixing rule. Markers show experimental data. Error bars have been omitted when the length of the error bar does not exceed the width of the marker. The pure-component viscosities for each simulation have been assigned as the experimental data points which are measured at as close to 0 mass fraction of water.

Table S5. Mean absolute error (MAE) and mean bias error (MBE) for AIOMFAC–VISC and the mole-fraction scaled mixing rule predictions of mixture viscosity of binary aqueous organic systems as compared to experimental data at $T = 293.15$ K (or the temperature indicated in the source column).

| | | η^0_{Best} | | | | | η^0_{DeRieux} | | | |
| | | AIOMFAC-VISC | | Mole Fraction | | | AIOMFAC-VISC | | Mole Fraction | |
System compound	Source	$\log_{10}\left[\frac{\eta^0_{\text{Best}}}{(\text{Pa s})}\right]$	MAE	MBE	MAE	MBE	$\log_{10}\left[\frac{\eta^0_{\text{DeRieux}}}{(\text{Pa s})}\right]$	MAE	MBE	MAE	MBE
1,2,4-butanetriol	Song et al. (2016)	0.2100	0.0152	0.0052	0.0174	-0.0171	1.0481	0.1757	0.1757	0.1300	0.1286
1,2,6-hexanetriol	Song et al. (2016)	0.5500	0.0371	-0.0363	0.0675	-0.0675	1.9845	0.3103	0.3083	0.2412	0.2286
1,4-butanediol	Song et al. (2016)	-1.0380	0.0034	0.0001	0.0040	-0.0022	-0.8571	0.0035	0.0032	0.0028	0.0002
1,4-butanediol	Yang et al. (2004)	-1.0380	0.0035	-0.0034	0.0044	-0.0043	-0.8571	0.0035	-0.0009	0.0042	-0.0023
citric acid	Haynes (2014)	7.9275	0.0000	0.0000	0.0000	0.0000	11.8101	0.0002	0.0002	0.0001	0.0001
citric acid	Song et al. (2016)	7.9275	0.4144	0.2829	0.4174	0.3460	11.8101	1.9579	1.9579	2.1932	2.1932
erythritol	Song et al. (2016)	2.9287	0.2921	-0.2915	0.3798	-0.3797	3.0174	0.2689	-0.2680	0.3574	-0.3573
fructose	Haynes (2014)	10.0678	0.0001	0.0001	0.0002	0.0002	8.7321	0.0001	0.0001	0.0001	0.0001
fructose	Rampp et al. (2000)	10.0678	0.0052	0.0021	0.0628	0.0628	8.7321	0.1001	-0.1000	0.0436	-0.0434
fructose	Telis et al. (2007)	10.0678	0.0002	-0.0002	0.0011	0.0011	8.7321	0.0004	-0.0002	0.0002	0.0002
fructose	Rampp et al. (2000) (at 283 K)	12.3570	0.0212	-0.0178	0.1459	0.1459	11.0057	0.1010	-0.1010	0.0231	-0.0003
fructose	Telis et al. (2007) (at 283 K)	12.3570	0.0005	-0.0003	0.0028	0.0028	11.0057	0.0008	-0.0007	0.0011	0.0011
glucose	Gladden and Dole (1953) (at 298 K)	12.9982	0.0495	0.0495	0.1572	0.1572	7.8215	0.0397	-0.0397	0.0312	-0.0312
glucose	Song et al. (2016)	13.7472	1.1186	-0.5425	0.7435	-0.1882	8.7321	1.9370	-1.9370	1.9554	-1.9554
glutaric acid	Song et al. (2016)	0.3115	0.0003	0.0003	0.0005	0.0003	3.7869	0.0102	0.0102	0.0155	0.0155
glycerol	Haynes (2014)	0.1482	0.0011	-0.0011	0.0051	-0.0051	0.6752	0.0172	0.0172	0.0119	0.0097
glycerol	Song et al. (2016)	0.1482	0.2547	-0.2547	0.2911	-0.2911	0.6752	0.1998	-0.0305	0.1484	-0.0945
maleic acid	Song et al. (2016)	-0.8640	0.0000	0.0000	0.0003	0.0003	4.1521	0.0077	0.0077	0.0074	0.0074
maltose	Song et al. (2016)	33.9582	1.4869	-1.4851	0.3022	0.0526	19.1178	1.9059	-1.9050	1.5884	-1.5877
raffinose	Song et al. (2016)	37.3558	2.2183	-2.1854	1.3521	-1.3391	27.7649	2.2912	-2.2593	2.0317	-2.0304
sorbitol	Song et al. (2016)	8.1737	0.5003	-0.2749	0.5245	-0.4059	8.6349	0.4966	-0.2018	0.5110	-0.3179
sucrose	Gladden and Dole (1953) (at 298 K)	15.8319	0.0175	-0.0161	0.0137	-0.0137	18.1038	0.0157	-0.0141	0.0120	-0.0120
sucrose	Quintas et al. (2006)	16.7816	1.0802	-1.0802	0.8105	-0.8105	19.2312	0.9963	-0.9963	0.4997	-0.4997
sucrose	Power et al. (2013)	16.7816	1.1108	-1.0195	0.7388	-0.6270	19.2312	0.9147	-0.7647	0.4301	-0.1345
sucrose	Telis et al. (2007)	16.7816	0.0010	0.0010	0.0011	-0.0011	19.2312	0.0011	0.0011	0.0005	-0.0005
sucrose	Haynes (2014)	16.7816	0.0025	-0.0009	0.0014	-0.0014	19.2312	0.0023	-0.0007	0.0008	-0.0008
sucrose	Song et al. (2016)	16.7816	1.3781	-0.1887	1.0439	0.1545	19.2312	1.6219	0.3743	1.4092	0.9672
sucrose	Swindells et al. (1958)	16.7816	0.0159	-0.0137	0.0138	-0.0138	19.2312	0.0151	-0.0128	0.0115	-0.0115
sucrose	Först et al. (2002)	16.7816	0.0010	0.0009	0.0014	-0.0014	19.2312	0.0010	0.0010	0.0006	-0.0006
trehalose	Song et al. (2016)	33.9582	1.8832	-1.8832	0.4835	0.3433	19.1178	2.4315	-2.4315	1.9298	-1.9298
trehalose	Sampedro et al. (2002)	33.9582	0.0002	0.0002	0.0002	0.0002	19.1178	0.0002	0.0002	0.0000	0.0000
trehalose	Galmarini et al. (2011)	33.9582	0.0007	0.0007	0.0013	0.0013	19.1178	0.0006	0.0006	0.0003	-0.0003
trehalose	Miller and Corti (1997)	33.9582	0.6097	-0.6097	0.0645	0.0547	19.1178	0.6237	-0.6237	0.6304	-0.6304
	Sum =		12.523	-9.562	7.654	-2.846	Sum =	16.452	-8.830	14.223	-6.089

All values are dimensionless numbers (magnitude closer to zero is better) based on $\log_{10}\left[(\text{Pa s})/(\text{Pa s})\right]$; refer to Eq. (S6).

η^0_{DeRieux}: pure-component viscosity of organic at stated T is calculated based on the DeRieux et al. (2018) method.

η^0_{Best}: pure-component viscosity or organic at stated T is assigned as the optimal value of all methods explored to determine the pure-component viscosity.

The fraction of systems where AIOMFAC-VISC outperforms the mole-fraction scaled mixing rule is 61 % in terms of MAE and 67 % in terms of MBE when using η^0_{Best}.

Not listed are the MAE and MBE for the activity-scaled mixing rule; however, the fraction of systems where AIOMFAC-VISC is the better model is 91% in terms of MAE and 94% in terms of MBE when using η^0_{Best}.
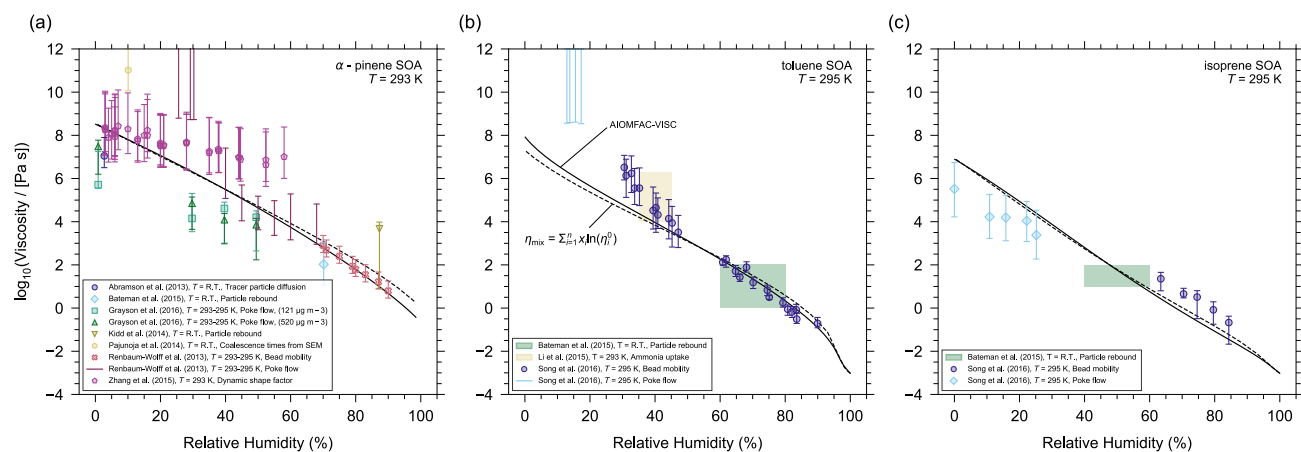
Figure S9. AIOMFAC–VISC mixture viscosity predictions for (**a**) α-pinene SOA at $T = 293$ K, (**b**) toluene SOA at $T = 295$ K, and (**c**) isoprene SOA at $T = 295$ K. The solid black lines are the AIOMFAC-VISC mixture viscosity prediction. The dashed black lines are the mixture viscosity prediction from the mole-fraction-weighted mixing rule. The markers and colour shaded regions represent experimental data obtained by different methods (see legend). $T = $ R.T. indicates the measurements were taken at room temperature ($\sim 293 \pm 4$ K). The same relative amounts of organics that are listed in Tables S2 – S4 are used for the simulations of both models.

References

Ablett, S., Izzard, M. J., Lillford, P. J., Arvanitoyannis, I., and Blanshard, J. M.: Calorimetric study of the glass transition occuring in fructose solutions, Carbohydrate Research, 246, 13–22, https://doi.org/10.1016/0008-6215(93)84020-7, 1993.

Angell, C.: Entropy and Fragility in Supercooling Liquids, vol. 102, https://doi.org/10.6028/jres.102.013, 1997.

5   Bodsworth, A., Zobrist, B., and Bertram, A. K.: Inhibition of efflorescence in mixed organic-inorganic particles at temperatures less than 250 K, Physical Chemistry Chemical Physics, 12, 12 259–12 266, https://doi.org/10.1039/c0cp00572j, 2010.

Böhmer, R., Ngai, K. L., Angell, C. A., and Plazek, D. J.: Nonexponential relaxations in strong and fragile glass formers, The Journal of Chemical Physics, 99, 4201–4209, https://doi.org/10.1063/1.466117, 1993.

Cao, W., Knudsen, K., Fredenslund, A., and Rasmussen, P.: Group-Contribution Viscosity Predictions of Liquid Mixtures Using UNIFAC-
10   VLE Parameters, Ind. Eng. Chem. Res., 32, 2088–2092, https://doi.org/10.1021/ie00021a034, 1993.

Compernolle, S., Ceulemans, K., and Muller, J. F.: EVAPORATION: a new vapour pressure estimation methodfor organic molecules including non-additivity and intramolecular interactions, Atmos. Chem. Phys., 11, 9431–9450, https://doi.org/10.5194/acp-11-9431-2011, <GotoISI>://WOS:000295368700001, 2011.

Dehaoui, A., Issenmann, B., and Caupin, F.: Viscosity of deeply supercooled water and its coupling to molecular diffusion, Proceedings of
15   the National Academy of Sciences, 112, 12 020–12 025, https://doi.org/10.1073/pnas.1508996112, 2015.

DeRieux, W. S. W., Li, Y., Lin, P., Laskin, J., Laskin, A., Bertram, A. K., Nizkorodov, S. A., and Shiraiwa, M.: Predicting the glass transition temperature and viscosity of secondary organic material using molecular composition, Atmospheric Chemistry and Physics, 18, 6331–6351, https://doi.org/10.5194/acp-18-6331-2018, 2018.

Dette, H. P., Qi, M., Schröder, D. C., Godt, A., and Koop, T.: Glass-forming properties of 3-methylbutane-1,2,3-tricarboxylic acid and its
20   mixtures with water and pinonic acid, Journal of Physical Chemistry A, 118, 7024–7033, https://doi.org/10.1021/jp505910w, 2014.

Dorfmüller, T., Dux, H., Fytas, G., and Mersch, W.: A light scattering study of the molecular motion in hexanetriol 1,2,6, The Journal of Chemical Physics, 71, 366–375, https://doi.org/10.1063/1.438079, 1979.

Först, P., Werner, F., and Delgado, A.: On the pressure dependence of the viscosity of aqueous sugar solutions, Rheologica Acta, 41, 369–374, https://doi.org/10.1007/s00397-002-0238-y, 2002.

25   Galmarini, M., Baeza, R., Sanchez, V., Zamora, M., and Chirife, J.: Comparison of the viscosity of trehalose and sucrose solutions at various temperatures: Effect of guar gum addition, LWT-Food Science and Technology, 44, 186–190, 2011.

Gladden, J. and Dole, M.: Diffusion in supersaturated solutions. II. Glucose solutions, Journal of the American Chemical Society, 75, 3900–3904, 1953.

Hancock, B. C., Shamblin, S. L., and Zografi, G.: Molecualr Mobility of Amorphous Pharmaceutical Solids Below Their Glass Transition
30   Temperatures, Pharmaceutical Research, 12, 799–806, 1995.

Haynes, W. M.: CRC handbook of chemistry and physics, CRC press, 2014.

Hoppu, P., Hietala, S., Schantz, S., and Juppo, A. M.: Rheology and molecular mobility of amorphous blends of citric acid and paracetamol, European Journal of Pharmaceutics and Biopharmaceutics, 71, 55–63, https://doi.org/10.1016/j.ejpb.2008.06.029, 2009.

Kawai, K., Hagiwara, T., Takai, R., and Suzuki, T.: Comparative investigation by two analytical approaches of enthalpy relaxation for glassy
35   glucose, sucrose, maltose, and trehalose, Pharmaceutical Research, 22, 490–495, https://doi.org/10.1007/s11095-004-1887-6, 2005.

Lienhard, D. M., Zobrist, B., Zuend, A., Krieger, U. K., and Peter, T.: Experimental evidence for excess entropy discontinuities in glass-forming solutions, Journal of Chemical Physics, 136, 74 515, https://doi.org/10.1063/1.3685902, 2012.

Lu, Q. and Zografi, G.: Properties of citric acid at the glass transition, Journal of Pharmaceutical Sciences, 86, 1374–1378, https://doi.org/10.1021/js970157y, 1997.

Marsh, A., Petters, S. S., Rothfuss, N. E., Rovelli, G., Song, Y. C., Reid, J. P., and Petters, M. D.: Amorphous phase state diagrams and viscosity of ternary aqueous organic/organic and inorganic/organic mixtures, Physical Chemistry Chemical Physics, 20, 15 086–15 097, https://doi.org/10.1039/c8cp00760h, 2018.

Miller, D.P., P. J. and Corti, H.: Thermophysical Properties of Trehalose and Its concentrated Aqueous Solutions, Pharmaceutical Research, 14, 578–590, https://doi.org/10.1023/A:1012192725996, 1997.

Murray, B. J.: Inhibition of ice crystallisation in highly viscous aqueous organic acid droplets, Atmospheric Chemistry and Physics, 8, 5423–5433, https://doi.org/10.5194/acp-8-5423-2008, 2008.

Nakanishi, M. and Nozaki, R.: Systematic study of the glass transition in polyhydric alcohols, Physical Review E - Statistical, Nonlinear, and Soft Matter Physics, 83, 51 503, https://doi.org/10.1103/PhysRevE.83.051503, 2011.

Nannoolal, Y., Rarey, J., Ramjugernath, D., and Cordes, W.: Estimation of pure component properties: Part 1. Estimation of the normal boiling point of non-electrolyte organic compounds via group contributions and group interactions, Fluid Phase Equilibria, 226, 45–63, https://doi.org/10.1016/j.fluid.2004.09.001, 2004.

Nannoolal, Y., Rarey, J., and Ramjugernath, D.: Estimation of pure component properties - Part 3. Estimation of the vapor pressure of non-electrolyte organic compounds via group contributions and group interactions, Fluid Phase Equilib., 269, http://dx.doi.org/10.1016/j.fluid.2008.04.020, 2008.

Nannoolal, Y., Rarey, J., and Ramjugernath, D.: Estimation of pure component properties. Part 4: Estimation of the saturated liquid viscosity of non-electrolyte organic compounds via group contributions and group interactions, Fluid Phase Equilibria, 281, 97–119, https://doi.org/10.1016/j.fluid.2009.02.016, 2009.

Ollet, A. L. and Parker, R.: The Viscosity of Supercooled Fructose and Its Glass Transition Temperature, Journal of Texture Studies, 21, 355–362, https://doi.org/10.1111/j.1745-4603.1990.tb00484.x, 1990.

Power, R. M., Simpson, S. H., Reid, J. P., and Hudson, A. J.: The transition from liquid to solid-like behaviour in ultrahigh viscosity aerosol particles, Chemical Science, 4, 2597–2604, https://doi.org/10.1039/c3sc50682g, 2013.

Quintas, M., Brandão, T. R., Silva, C. L., and Cunha, R. L.: Rheology of supersaturated sucrose solutions, Journal of Food Engineering, 77, 844–852, https://doi.org/10.1016/j.jfoodeng.2005.08.011, 2006.

Rampp, M., Buttersack, C., and Lüdemann, H.-D.: c,T-Dependence of the viscosity and the self-diffusion coefficients in some aqueous carbohydrate solutions, Carbohydrate Research, 328, 561–572, https://doi.org/10.1016/S0008-6215(00)00141-5, 2000.

Rastak, N., Pajunoja, A., Acosta Navarro, J. C., Ma, J., Song, M., Partridge, D. G., Kirkevåg, A., Leong, Y., Hu, W. W., Taylor, N. F., Lambe, A., Cerully, K., Bougiatioti, A., Liu, P., Krejci, R., Petäjä, T., Percival, C., Davidovits, P., Worsnop, D. R., Ekman, A. M. L., Nenes, A., Martin, S., Jimenez, J. L., Collins, D. R., Topping, D. O., Bertram, A. K., Zuend, A., Virtanen, A., and Riipinen, I.: Microphysical explanation of the RH-dependent water affinity of biogenic organic aerosol and its importance for climate, Geophys. Res. Lett., 44, 5167–5177, https://doi.org/10.1002/2017GL073056, https://doi.org/10.1002/2017GL073056, 2017.

Renbaum-Wolff, L., Grayson, J. W., Bateman, A. P., Kuwata, M., Sellier, M., Murray, B. J., Shilling, J. E., Martin, S. T., and Bertram, A. K.: Viscosity of -pinene secondary organic material and implications for particle growth and reactivity, Proceedings of the National Academy of Sciences, 110, 8014–8019, https://doi.org/10.1073/pnas.1219548110, 2013.

Rothfuss, N. E. and Petters, M. D.: Influence of Functional Groups on the Viscosity of Organic Aerosol, Environmental Science and Technology, 51, 271–279, https://doi.org/10.1021/acs.est.6b04478, 2017.

Sampedro, J. G., Munoz-Clares, R. A., and Uribe, S.: Trehalose-mediated inhibition of the plasma membrane H+-ATPase from Kluyveromyces lactis: dependence on viscosity and temperature, Journal of bacteriology, 184, 4384–4391, 2002.

Seidl, M., Loerting, T., Bohmer, R., Gainaru, C., Nelson, H., Amann-Winkel, K., and Handle, P. H.: Water's second glass transition, Proceedings of the National Academy of Sciences, 110, 17 720–17 725, https://doi.org/10.1073/pnas.1311718110, 2013.

5 Simatos, D., Blond, G., Roudaut, G., Champion, D., Perez, J., and Faivre, A. L.: Influence of heating and cooling rates on the glass transition temperature and the fragility parameter of sorbitol and fructose as measured by DSC, Journal of Thermal Analysis, 47, 1419–1436, https://doi.org/10.1007/BF01992837, 1996.

Simperler, A., Kornherr, A., Chopra, R., Bonnet, P. A., Jones, W., Motherwell, W. D., and Zifferer, G.: Glass transition temperature of glucose, sucrose, and trehalose: An experimental and in silico study, Journal of Physical Chemistry B, 110, 19 678–19 684,

10 https://doi.org/10.1021/jp063134t, 2006.

Song, M., Liu, P. F., Hanna, S. J., Zaveri, R. A., Potter, K., You, Y., Martin, S. T., and Bertram, A. K.: Relative humidity-dependent viscosity of secondary organic material from toluene photo-oxidation and possible implications for organic particulate matter over megacities, Atmospheric Chemistry and Physics, 16, 8817–8830, https://doi.org/10.5194/acp-16-8817-2016, 2016.

Swindells, J., Snyder, C., Hardy, R., and Golden, P.: Viscosities of sucrose solutions at various temperatures: Tables of recalculated values,

15 https://doi.org/10.1016/S0016-7037(03)00105-4, 1958.

Telis, V. R., Telis-Romero, J., Mazzotti, H. B., and Gabas, A. L.: Viscosity of aqueous carbohydrate solutions at different temperatures and concentrations, International Journal of Food Properties, 10, 185–195, https://doi.org/10.1080/10942910600673636, 2007.

Timko, R. J. and Lordi, N. G.: Thermal characterization of citric acid solid dispersions with benzoic acid and phenobarbital, in: Journal of Pharmaceutical Sciences, vol. 68, pp. 601–605, Elsevier, https://doi.org/10.1002/jps.2600680523, https://www.sciencedirect.com/science/

20 article/pii/S0022354915426504, 1979.

Viswanath, D. S., Ghosh, T. K., Prasad, D. H. L., Dutt, N. V., and Rani, K. Y.: Viscosity of Liquids, Springer, 2007.

Yang, C., Ma, P., and Zhou, Q.: Excess Molar Volume, Viscosity, and Heat Capacity for the Mixtures of 1,4-Butanediol + Water at Different Temperatures, Journal of Chemical and Engineering Data, 49, 582–587, https://doi.org/10.1021/je0341918, 2004.

Zhang, Y., Katira, S., Lee, A., Lambe, A. T., Onasch, T. B., Xu, W., Brooks, W. A., Canagaratna, M. R., Freedman, A., Jayne, J. T., Worsnop,

25 D. R., Davidovits, P., Chandler, D., and Kolb, C. E.: Kinetically controlled glass transition measurement of organic aerosol thin films using broadband dielectric spectroscopy, Atmospheric Measurement Techniques, 11, 3479–3490, https://doi.org/10.5194/amt-11-3479-2018, 2018.

Zobrist, B., Marcolli, C., Pedernera, D. A., and Koop, T.: Do atmospheric aerosols form glasses?, Atmospheric Chemistry and Physics, 8, 5221–5244, https://doi.org/10.5194/acp-8-5221-2008, 2008.

30 Zuend, A. and Seinfeld, J. H.: Modeling the gas-particle partitioning of secondary organic aerosol: The importance of liquid-liquid phase separation, Atmospheric Chemistry and Physics, 12, 3857–3882, https://doi.org/10.5194/acp-12-3857-2012, 2012.

Zuend, A., Marcolli, C., Booth, A. M., Lienhard, D. M., Soonsin, V., Krieger, U. K., Topping, D. O., McFiggans, G., Peter, T., and Seinfeld, J. H.: New and extended parameterization of the thermodynamic model AIOMFAC: Calculation of activity coefficients for organic-inorganic mixtures containing carboxyl, hydroxyl, carbonyl, ether, ester, alkenyl, alkyl, and aromatic functional groups, Atmospheric

35 Chemistry and Physics, 11, 9155–9206, https://doi.org/10.5194/acp-11-9155-2011, 2011.